Level-spacing statistics and spectral correlations in diffuse van der Waals clusters

S. K. Haldar,[1] B. Chakrabarti,[2,*] N. D. Chavda,[3] T. K. Das,[4] S. Canuto,[5] and V. K. B. Kota[6]

[1]*Department of Physics, Lady Brabourne College, P-1/2 Suhrawardi Avenue, Kolkata-700017, India*

[2]*Department of Physics, Kalyani University, Kalyani, Nadia 741235, West Bengal, India*

[3]*Applied Physics Department, Faculty of Technology and Engineering, Maharaja Sayajirao University of Baroda, Vadodara 390 001, India*

[4]*Department of Physics, Calcutta University, 92 A. P. C. Road, Kolkata-700009, India*

[5]*Instituto de Fisica, Universidade of São Paulo, CP 66318, 05315-970, São Paulo, Brazil*

[6]*Physical Research Laboratory, Navarangpura, Ahmedabad 380009, India*

(Received 11 November 2013; published 9 April 2014)

We present a statistical analysis of eigenenergies and discuss several measures of spectral fluctuations and spectral correlations for the van der Waals clusters of different sizes. We show that the clusters become more and more complex with increase in cluster size. We study nearest-neighbor level-spacing distribution $P(s)$, the level number variance $\Sigma^2(L)$, and the Dyson-Mehta Δ_3 statistics for various cluster sizes. For large clusters we find that although the Bohigas-Giannoni-Schmit conjecture seems to be valid, it does not exhibit true signatures of quantum chaos. However, contrasting conjecture of Berry and Tabor is observed with smaller cluster size. For a small number of bosons, we observe the existence of a large number of quasidegenerate states in low-lying excitation which exhibits the Shnirelman peak in $P(s)$ distribution. We also find a narrow region of intermediate spectrum which can be described by semi-Poisson statistics whereas the higher levels are regular and exhibit Poisson statistics. These observations are further supported by the analysis of the distribution of the ratio of consecutive level spacings $P(r)$ which is independent of unfolding procedure and thereby provides a tool for more transparent comparison with experimental findings than $P(s)$. Thus our detail numerical study clearly shows that the van der Waals clusters become more correlated with the increase in cluster size.

DOI: 10.1103/PhysRevA.89.043607 PACS number(s): 03.75.Hh, 05.30.Jp, 05.45.Mt, 05.45.Tp

I. INTRODUCTION

Weakly bound few-body systems are being studied from a long time back and have achieved a revival of interest recently as the physics of such weakly bound systems can be investigated experimentally in ultracold atomic gases [1]. Utilizing the Feshbach resonance, the effective interatomic interaction can be changed essentially to any desired values [2,3]. The recent experiments on cold atoms also provide evidence of the existence of large weakly bound clusters. Thus our present study is motivated by the recent experiments on ultracold Bose gas. We treat the three-dimensional bosonic cluster with maximum up to $N = 40$ Rb atoms interacting through two-body van der Waals potential. Alkali-metal atoms, especially Rb atoms, are good candidates for laser manipulation and for observing Bose-Einstein condensate (BEC) [4]. At ultracold temperature the interatomic interaction is fairly well represented by a single parameter a_s, the s-wave scattering length. For our present system we keep $a_s = 100a_0$ which corresponds to the JILA experiment [4]. Thus the system is weakly interacting, and diffuse as the average size of the cluster increases with cluster size. The binding of such an N-body cluster is provided by the two-body van der Waals potential having a short-range repulsive core below a cutoff radius and a $\frac{-C_6}{r^6}$ tail which represents the long-range attractive interaction.

The stability of such N-body clusters, their energetics, and various structural properties are recently studied [5]. We propose the use of a two-body basis function to describe various properties of bosonic clusters. With more than three particles the system becomes more complex as the number of degrees of freedom increases. We have investigated correlations between energies of the N and $(N-1)$ systems and observe the generalized Tjon line [5] for the large cluster. Now we consider the spectral statistics and spectral correlation of the atomic clusters of different sizes as these contain rich physics and also play a pivotal role in establishing the universal properties of quantum systems. Berry and Tabor conjectured that the fluctuation property of the energy levels of a quantum system whose classical analog is regular, is characterized by Poisson statistics [6]. Whereas the fluctuation property of the energy levels of a quantum system whose corresponding classical dynamical system is fully chaotic obeys the Bohigas-Giannoni-Schmit (BGS) conjecture [7]. This tells that Gaussian orthogonal ensemble (GOE) or Gaussian unitary ensemble (GUE) or Gaussian sympletic ensemble (GSE) statistics of random matrix theory, depending on time-reversal symmetry and rotational symmetry of the system, will describe the fluctuation properties. However, this conjecture is often interpreted in another way and the observation of level repulsion in the spectrum is treated as an indication of the nonintegrability of the system. The Poisson distribution implies complete randomness in the relative positions of energy levels as they are completely uncorrelated. On the other hand Wigner distribution implies strong correlation among the energy levels.

Earlier the spectral properties of many different quantum systems like atoms, atomic nuclei, and quantum billiards have been studied [8–16]. In addition, some attempts have been made for noninteracting many-boson systems and interacting bosonic systems [17–20]. Recently we have reported the level-spacing distribution of ultracold interacting bosons trapped in a harmonic potential [21–23]. We found an intriguing

*Present address: Department of Physics, Presidency University, 86/1 College Street, Kolkata 700073, India.

effect of both the interatomic interaction and the trap and observed deviation from the BGS conjecture. In this paper we are interested in a similar type of calculation in the van der Waals bosonic clusters. Unlike the Bose-Einstein condensate where the external trapping provides the stability of the condensate, the van der Waals clusters are bound due to the van der Waals interaction. In the very dilute condition one may treat it as a uniform Bose gas. Apart from the experimental interest, these kinds of systems are also challenging for the following reasons. First, solving the many-body Schrödinger equation itself is a challenging numerical task due to many degrees of freedom, and the obvious question is what kind of approximation will be valid for the description of such clusters. Secondly, for large cluster size when the system becomes very much correlated, one may expect a Wigner-type spectral distribution. However, this needs an exhaustive study as level repulsion in the energy spectrum may not always lead to Wigner distribution which signifies chaos. This indicates that one may need to use some deformed GOE type of distribution for the correct description of a nonintegrable but nonchaotic system. We propose to study several measures of spectral fluctuations and spectral correlation to determine the degree of influence of the interatomic interaction. This kind of study is also relevant as the statistical fluctuation can be directly observed experimentally in the context of ultracold Bose gases. We calculate nearest neighbor level-spacing distribution (NNSD) $P(s)$, the level number variance $\Sigma^2(L)$, and the Dyson-Mehta Δ_3 statistics [24] for various cluster sizes. However, all these measures require unfolding of the spectrum to remove variation in the density-of-energy levels in different parts of the spectrum. We can either unfold the spectrum of each member of the ensemble separately and form ensemble-averaged NNSD or a single unfolding function can be used for all the members of the ensemble. Depending on the unfolding procedure, the final outcome of NNSD may vary. Moreover, a suitable unfolding function is not always known *a priori* and generally is approximated by higher order polynomials. Therefore, to verify the outcome of the NNSD, we further analyze the distribution of quotients of successive spacings $P(r)$ which does not require any unfolding and is independent of the energy level density.

The paper is organized as follows. In Sec. II, we introduce the many-body potential harmonic expansion method. Section III discusses the numerical results and Sec. IV concludes with the summary of our work.

II. METHODOLOGY: MANY-BODY CALCULATION WITH POTENTIAL HARMONIC BASIS

To study the spectral statistics and different spectral correlations we need to calculate a large number of energy levels of the diffuse Rb cluster. We approximately solve the full many-body Schrödinger equation by our recently developed potential harmonic expansion method. We have earlier applied it successfully to study different properties of BEC [25–31] and atomic clusters [5,32,33]. The methodology has already been described in detail in our earlier works [34–36]. Hence here we describe it briefly for interested readers.

We consider a system of $N = (\mathcal{N}+1)$ Rb atoms, each of mass m and interacting via two-body potential. The time-independent quantum many-body Schrödinger equation is given by

$$\left[-\frac{\hbar^2}{2m}\sum_{i=1}^{N}\nabla_i^2+\sum_{i,j>i}^{N}V(\vec{r}_i-\vec{r}_j)-E\right]\Psi(\vec{r}_1,\ldots,\vec{r}_N)=0, \tag{1}$$

where E is the total energy of the system, $V(\vec{r}_i-\vec{r}_j)$ is the two-body potential, and $\vec{r}_i$ is the position vector of the ith particle. It is usual practice to decompose the motion of a many-body system into the motion of the center of mass and the relative motion of the particles in the center-of-mass frame. In the absence of any confining potential the center of mass behaves as a free particle in the laboratory frame and we set its energy as zero. Hence, after elimination of the center-of-mass motion and using standard Jacobi coordinates, defined as [37–39]

$$\vec{\zeta}_i=\sqrt{\frac{2i}{i+1}}\left(\vec{r}_{i+1}-\frac{1}{i}\sum_{j=1}^{i}\vec{r}_j\right)\quad(i=1,\ldots,\mathcal{N}), \tag{2}$$

we obtain the equation for the relative motion of the atoms,

$$\left[-\frac{\hbar^2}{m}\sum_{i=1}^{\mathcal{N}}\nabla_{\zeta_i}^2+V_{\rm int}(\vec{\zeta}_1,\ldots,\vec{\zeta}_{\mathcal{N}})-E\right]\Psi(\vec{\zeta}_1,\ldots,\vec{\zeta}_{\mathcal{N}})=0\,. \tag{3}$$

$V_{\rm int}$ is the sum of all pairwise interactions. Now it is to be noted that the hyperspherical harmonic expansion method is an *ab initio* tool to solve the many-body Schrödinger equation where the total wave function is expanded in the complete set of the hyperspherical basis [37]. Although the hyperspherical harmonic expansion method is a complete many-body approach and includes all possible correlations, it is highly restricted to $N=3$ only. But for a diffuse cluster like the Rb cluster, only two-body correlation and pairwise interaction are important. Therefore, we can decompose the total wave function Ψ into the two-body Faddeev component for the interacting (ij) pair as

$$\Psi=\sum_{i,j>i}^{N}\phi_{ij}(\vec{r}_{ij},r). \tag{4}$$

It is important to note that ϕ_{ij} is a function of two-body separation $(\vec{r}_{ij})$ only and the global hyperradius r, which is defined as $r=\sqrt{\sum_{i=1}^{N}\zeta_i^2}$. Thus the effect of two-body correlation comes through the two-body interaction in the expansion basis. ϕ_{ij} is symmetric under the exchange operator P_{ij} for bosonic atoms and satisfies the Faddeev equation,

$$[T-E_R]\,\phi_{ij}=-V(\vec{r}_{ij})\sum_{kl>k}^{N}\phi_{kl}, \tag{5}$$

where T is the total kinetic energy operator. In this approach, we assume that when the (ij) pair interacts, the rest of the bosons are inert spectators. Thus, the total hyperangular momentum quantum number, as also the orbital angular momentum of the whole system, is contributed to by the interacting pair only. Next the (ij)th Faddeev component

is expanded in the set of potential harmonics (PH) [which is a subset of the hyperspherical harmonic (HH) basis and sufficient for the expansion of $V(\vec{r}_{ij})$] appropriate for the (ij) partition as

$$\phi_{ij}(\vec{r}_{ij},r) = r^{-(\frac{3\mathcal{N}-1}{2})} \sum_K \mathcal{P}^{lm}_{2K+l}\left(\Omega^{ij}_{\mathcal{N}}\right) u^l_K(r). \tag{6}$$

$\Omega^{ij}_{\mathcal{N}}$ denotes the full set of hyperangles in the $3\mathcal{N}$-dimensional space corresponding to the (ij) interacting pair and $\mathcal{P}^{lm}_{2K+l}(\Omega^{ij}_{\mathcal{N}})$ is called the PH. It has an analytic expression:

$$\mathcal{P}^{l,m}_{2K+l}\left(\Omega^{(ij)}_{\mathcal{N}}\right) = Y_{lm}(\omega_{ij})\ {}^{(\mathcal{N})}P^{l,0}_{2K+l}(\phi)\mathcal{Y}_0(D-3);\quad D = 3\mathcal{N}, \tag{7}$$

$\mathcal{Y}_0(D-3)$ is the HH of order zero in the $(3\mathcal{N}-3)$-dimensional space spanned by $\{\vec{\zeta}_1,\ldots,\vec{\zeta}_{\mathcal{N}-1}\}$ Jacobi vectors; ϕ is the hyperangle between the $\mathcal{N}$th Jacobi vector $\vec{\zeta}_{\mathcal{N}} = \vec{r}_{ij}$ and the hyperradius r and is given by $\zeta_{\mathcal{N}} = r\cos\phi$. For the remaining $(\mathcal{N}-1)$ noninteracting bosons we define hyperradius as

$$\rho_{ij} = \sqrt{\sum_{K=1}^{\mathcal{N}-1}\zeta_K^2} = r\sin\phi, \tag{8}$$

such that $r^2 = r_{ij}^2 + \rho_{ij}^2$. The set of $(3\mathcal{N}-1)$ quantum numbers of HH is now reduced to *only* 3 as for the $(\mathcal{N}-1)$ noninteracting pair,

$$l_1 = l_2 = \ldots = l_{\mathcal{N}-1} = 0, \tag{9}$$

$$m_1 = m_2 = \ldots = m_{\mathcal{N}-1} = 0, \tag{10}$$

$$n_2 = n_3 = \ldots n_{\mathcal{N}-1} = 0, \tag{11}$$

and for the interacting pair $l_{\mathcal{N}} = l$, $m_{\mathcal{N}} = m$, and $n_{\mathcal{N}} = K$. Thus the $3\mathcal{N}$-dimensional Schrödinger equation reduces effectively to a four-dimensional equation with the relevant set of quantum numbers: energy E, orbital angular momentum quantum number l, azimuthal quantum number m, and grand orbital quantum number $2K+l$ for any N. Substituting in Eq. (4) and projecting on a particular PH, a set of coupled differential equation for the partial wave $u^l_K(r)$ is obtained:

$$\left[-\frac{\hbar^2}{m}\frac{d^2}{dr^2} + \frac{\hbar^2}{mr^2}\{\mathcal{L}(\mathcal{L}+1) + 4K(K+\alpha+\beta+1)\} - E_R\right]U_{Kl}(r) + \sum_{K'} f_{Kl}V_{KK'}(r)f_{K'l}U_{K'l}(r) = 0, \tag{12}$$

where $\mathcal{L} = l + \frac{3N-6}{2}$, $U_{Kl} = f_{Kl}u^l_K(r)$, $\alpha = \frac{3N-8}{2}$, and $\beta = l + 1/2$.

f_{Kl} is a constant and represents the overlap of the PH for the interacting partition with the sum of PHs corresponding to all partitions [39]. The potential matrix element $V_{KK'}(r)$ is given by

$$V_{KK'}(r) = \int P^{lm^*}_{2K+l}\left(\Omega^{ij}_{\mathcal{N}}\right)V(r_{ij})P^{lm}_{2K'+1}\left(\Omega^{ij}_{\mathcal{N}}\right)d\Omega^{ij}_{\mathcal{N}}. \tag{13}$$

Here we would like to point out that we did not require the additional short-range correlation function $\eta(r_{ij})$ for Rb clusters as was necessary for dilute BEC. A BEC is designed to be very dilute and hence confined by a harmonic oscillator potential of low frequency (∼100 Hz). The average interatomic separation is thus very large (∼20000a_0) compared with the range of atom-atom interaction (∼100a_0). Moreover, the kinetic energy of the atoms is extremely small. Hence the effective interaction for large r_{ij} is controlled by the s-wave scattering length (a_s) [40]. This is achieved by the inclusion of the correlation function [35,36]. On the other hand, diffuse van der Waals clusters are weakly bound by the actual interatomic van der Waals potential (of range ∼ 10a_0), without any confinement. Hence no correlation function is needed. The average interparticle separation is large enough, so that only two-body correlations are expected to be adequate, at least for light clusters.

III. RESULTS

A. Choice of interaction and calculation of many-body effective potential

As pointed out earlier we choose the van der Waals potential with a hard core of radius r_c as the interaction potential, $V(r_{ij}) = \infty$ for $r_{ij} \leqslant r_c$ and $= -\frac{C_6}{r_{ij}^6}$ for $r_{ij} > r_c$. For Rb atoms, the value of C_6 is 2803 eV Å^6 [40]. The unmanipulated scattering length corresponding to the Rb dimer is $a_s = 100a_0$. We obtain a_s by solving the two-body Schrödinger equation for zero energy [36]. We adjust the hard core radius in the two-body equation to obtain the dimer scattering length. In Fig. 1 of Ref. [36], we see the value of a_s changes from negative to positive passing through an infinite discontinuity as r_c decreases. Each discontinuity corresponds to one extra two-body bound state. We observe that tiny change in r_c across the infinite discontinuity causes a_s to jump from very large positive value to very large negative value. For our present calculation, we tune r_c such that it corresponds to the single bound state of the dimer. Thus calculated r_c is 15.18 Å for the dimer scattering length of Rb atoms. With this set of values of C_6 and r_c, we next solve the coupled differential equation [12] by hyperspherical adiabatic approximation [41]. In hyperspherical adiabatic approximation, the hyperradial motion is assumed slow compared to hyperangular motion. For the hyperangular motion for a fixed value of r, we diagonalize the potential matrix together with the hypercentrifugal term. Thus the effective potential for the hyperradial motion is obtained as a parametric function of r. For the ground state of the system we choose the lowest eigenpotential $\omega_0(r)$ [corresponding eigencolumn vector being $\chi_{K0}(r)$] as the effective potential. We plot the effective potential $\omega_0(r)$ as a function of hyperradius r, at the dimer scattering length and for various cluster size $N = 3$, 5, and 40 in Fig. 1.

With an increase in cluster size the depth of the eigenpotential increases sharply which indicates stronger binding of the cluster. The average size of the cluster also increases with increases in N. The energy of the cluster is finally obtained by solving the adiabatically separated hyperradial equation in the extreme adiabatic approximation,

$$\left[-\frac{\hbar^2}{m}\frac{d^2}{dr^2} + \omega_0(r) - E_R\right]\zeta_0(r) = 0, \tag{14}$$

subject to appropriate boundary condition.

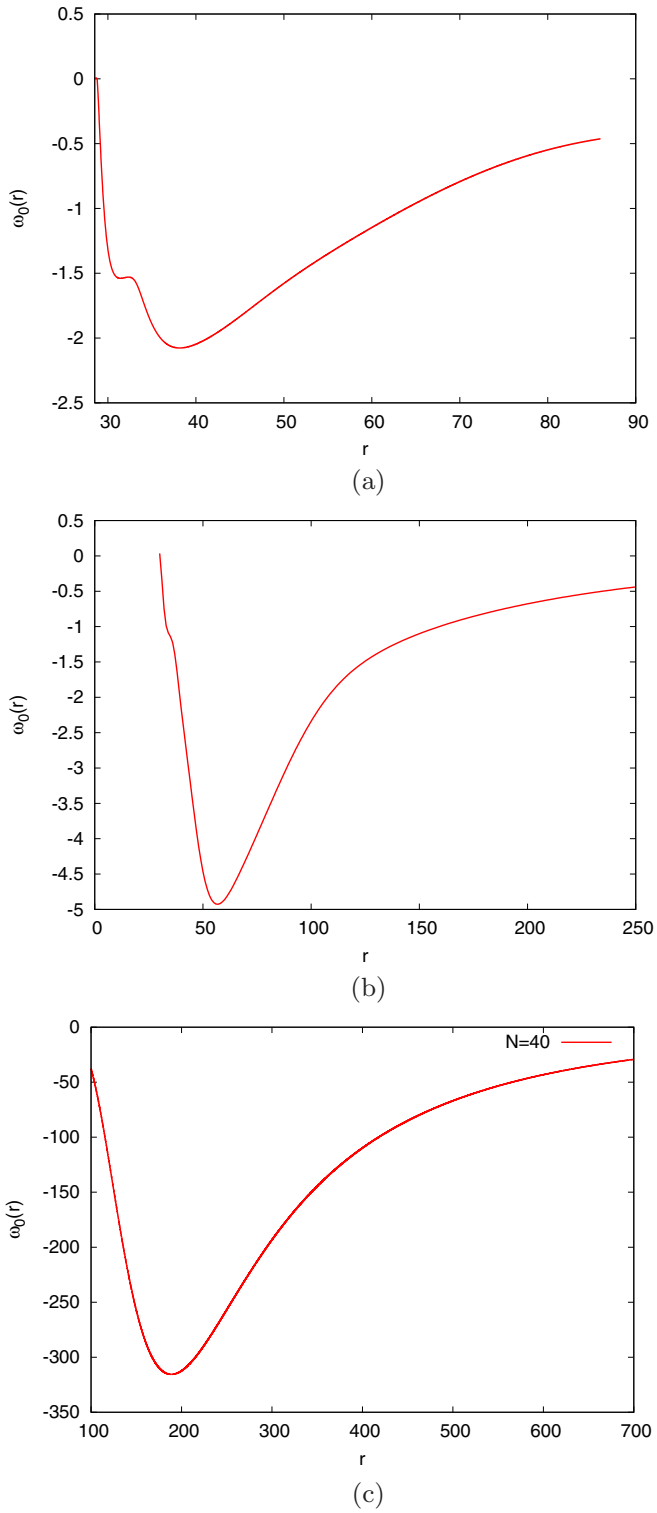

FIG. 1. (Color online) Plot of the effective potential $\omega_0(r)$ for different cluster sizes, *viz.* $N = 3$ (a), $N = 5$ (b), and $N = 40$ (c).

In our earlier published work we have reported ground-state and few low-lying excitations of the Rb cluster with maximum size of $N = 40$. [5]. However, in the calculation of level statistics and spectral correlation we also need higher multipolar excitations. In our many-body picture the collective motion of the cluster is described by the effective potential. The excited states in this potential are denoted by E_{nl} which corresponds to nth radial excitation with lth surface mode. Thus E_{00} corresponds to the ground state and E_{n0} are the different excitations for $l = 0$. To calculate the higher levels with $l \neq 0$ we follow the next procedure. We have noted that for $l \neq 0$, a large inaccuracy is involved in the calculation of the off-diagonal potential matrix. As the main contribution to the potential matrix comes from the diagonal hypercentrifugal term we disregard the contribution coming from the off-diagonal part. Thus we get the effective potential $\omega_l(r)$ for $l \neq 0$. Substituting $\omega_l(r)$ in Eq. (14) we solve for different radial modes and repeat the numerical procedure for various l to obtain the higher multipolar excitations.

Before discussing the statistical behavior of the energy spectrum we should discuss how accurate our calculated energy levels are. It is to be noted that the potential harmonic expansion method has been successfully applied in the calculation of collective excitations and thermodynamic properties of trapped bosons [42]. For the investigation of thermodynamic properties we need to calculate a large number of energy levels. The calculated critical temperature and the condensate fraction are in good agreement with the experimental results [42]. The effect of two-body correlations on thermodynamic properties of trapped bosons is also observed [42]. Very recently we have also studied the energetics of diffuse ^{87}Rb clusters [5] and also compared with the well-studied He, Ne, and Ar clusters. Thus the calculated energy levels are accurate for further analysis. We also check for the convergence such that the error is considerably smaller than the mean level spacings.

B. Level-spacing statistics for different cluster sizes

NNSD or $P(s)$ distribution is the most common observable which is used to study the short-range fluctuation. Now to compare the statistical property of different parts of the spectrum we need to unfold them. By unfolding, the smooth part of the level density is removed; it basically maps the energy levels to another with the mean level density equal to 1. For our present calculation we use polynomial unfolding of sixth order. We observe that for small cluster size with $N = 3$ and $N = 5$, as the effective potential is very shallow, the number of energy levels is very small and not sufficient for the calculation of NNSD. Instead, we also calculate the many-body collective levels including higher order excitations with different l. We then unfold each spectrum separately for a specific value of l and then form an ensemble having the same symmetry. From the unfolded spectrum we calculate the nearest neighbor spacing s as $E_{i+1} - E_i$ and calculate $P(s)$. $P(s)$ is defined as the probability density of finding a distance s between two adjacent levels. Uncorrelated spectra obey the Poisson statistics which gives exponential distribution $P(s) = e^{-s}$. Whereas for the system with time-reversal symmetry, level repulsion leads to the Wigner-Dyson distribution $P(s) = \frac{\pi}{2} s e^{\frac{-\pi s^2}{4}}$ [43].

The $P(s)$ distribution of the unfolded spectrum with cluster size $N = 3$ is plotted in Fig. 2. We observe that $P(s) = 0$ for very small s and also for large s. In our earlier calculation of the ^{87}Rb diffuse cluster, we have calculated the several low-energy excitations. We have observed that due to the heavier mass of Rb atom, the kinetic energy $\langle T \rangle$ of Rb_N clusters is small while

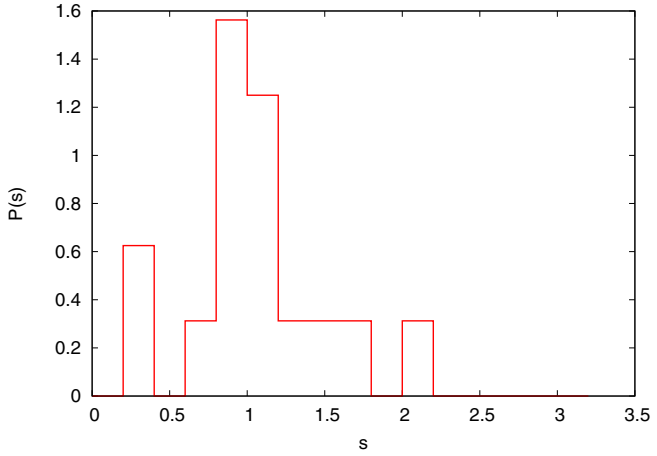

(a)

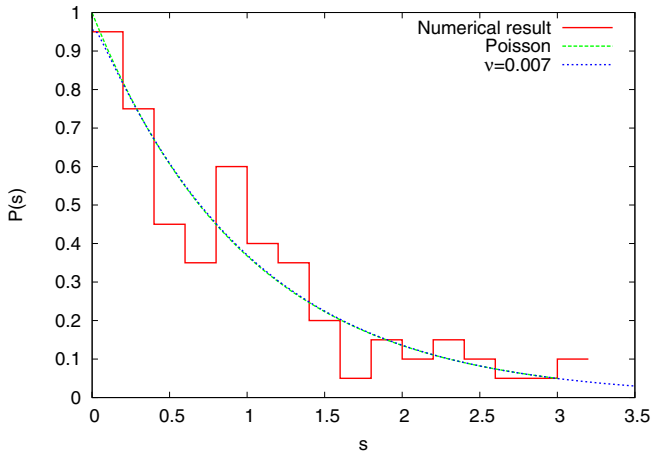

(b)

FIG. 2. (Color online) Plot of $P(s)$ distribution of (a) lowest 22 levels and (b) higher part of the spectrum (300 < levels < 400) of the diffuse ^{87}Rb cluster for $N = 3$. The green dashed curve in panel (b) represents the Poisson distribution whereas the blue dotted curve corresponds to the Brody distribution with the Brody parameter being $\nu = 0.007$.

the interaction energy $\langle V \rangle$ is large. This implies that although the system is tightly bound, it is less correlated for smaller N. Thus unlike the trapped bosons, the smaller diffuse cluster does not exhibit any degeneracy in the calculation of low-lying excitations. It is reflected in Fig. 2(a) where we observe that $P(s) = 0$ for very small s. The level spacing distribution for higher levels is shown in Fig. 2(b) which indicates that for such a small cluster, the energy levels are completely uncorrelated. Although it looks very similar to the Poisson distribution the peak value at $s = 0$ is less than 1. To determine how closely the histogram matches with the Poisson distribution we fit it with the Brody distribution [14],

$$P(\nu,s) = (1+\nu)as^{\nu}\exp(-as^{1+\nu}), \tag{15}$$

where $a = [\Gamma(\frac{2+\nu}{1+\nu})]^{1+\nu}$ and ν is the Brody parameter. Depending on the value of the Brody parameter ν, this distribution interpolates between the Poisson distribution ($\nu = 0$) and the Wigner distribution ($\nu = 1$). Here we found $\nu = 0.007$. This implies that there is negligible correlation between the

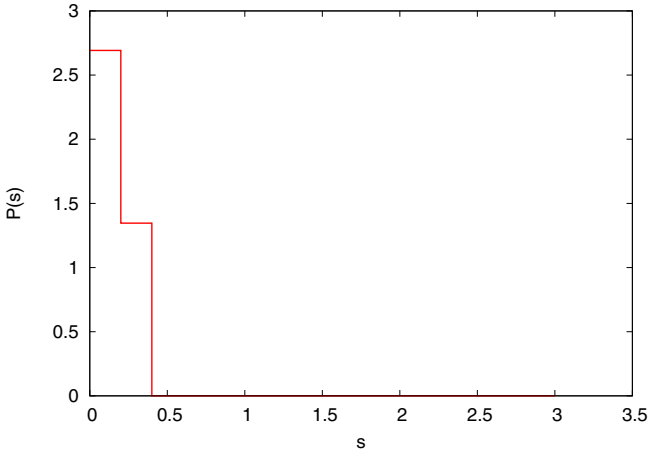

FIG. 3. (Color online) Plot of the $P(s)$ distribution of the lowest 30 levels of the ^{87}Rb cluster for $N = 5$.

energy levels and the system is very close to regular. Actually for $N = 3$ there are only three interacting pairs and the net attractive interaction is very weak.

Next to study the effect of interatomic interaction we gradually increase the effective interaction. We can vary the effective interaction either by tuning the scattering length a_s or by changing the number of bosons. Here we increase the number of bosons to $N = 5$. It is already known from the earlier study of the ^{4}He cluster that $\Delta E = E_{N+1} - E_N$ decreases smoothly as a function of N which indicates the saturation in the density and predicts liquid-drop behavior in the ^{4}He cluster with larger N [5]. However, the diffuse Rb cluster which is the system of our present interest is dilute and less compact which indicates a sharp change in ΔE with a change in cluster size. The average size of the cluster also increases. Thus the cluster with $N = 5$ is more tightly bound, stable, and more correlated compared with the cluster size $N = 3$. Due to more correlation in the energy spectrum, we can expect the very closely spaced energy levels which leads to the quasidegeneracy. This is reflected in Fig. 3 where we plot the $P(s)$ distribution for the lowest 30 levels. The sharp peak in the first bin near $s = 0$ clearly exhibits the signature of quasidegeneracy. This peak is known as the Shnirelman peak [44].

For a better understanding of the structure of the Shnirelman peak, we plot the same histogram in Fig. 4 as in Fig. 3 in finer details. Reducing the bin size gradually, a huge peak appears in the first bin which demonstrates the existence of global quasidegeneracy. The peak has a finite width which is further associated with the Poisson tail. The resolution of the peak is further studied as the integral level-spacing distribution $I(s) = N P(s)$ (here N being the number of levels), normalized to unity. We plot $I(s)$ as a function of $\ln s$ in Fig. 5. The linear dependence between I and $\ln s$ is shown in the leftmost part of Fig. 5 which represents the structure of the Shnirelman peak, whereas the rightmost steep increase of $I(s)$ corresponds to the Poisson tail. However, for the higher levels we observe that the system exhibits pseudointegrability. It is reflected in Fig. 6(a) where we observe the semi-Poisson (SP) distribution. For comparison, in the same figure we plot the analytic

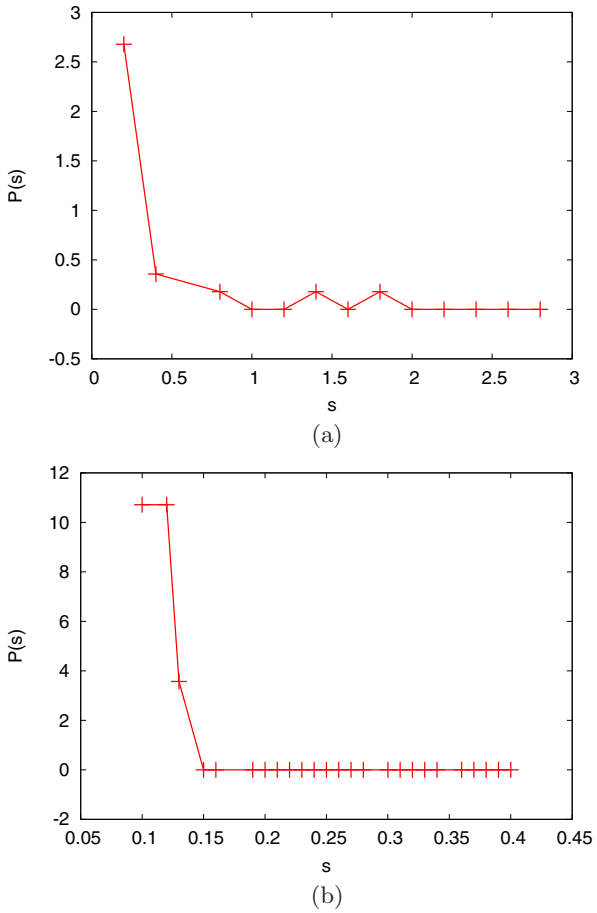

FIG. 4. (Color online) The structure of the Shnirelman peak observed for the lowest 30 levels of the ^{87}Rb cluster with $N = 5$ is shown in finer detail. The bin size in panel (a) is 0.2. In panel (b) only the peak is further zoomed by taking the bin size 0.01.

expression of SP statistics given by $P(s) = 4se^{-2s}$ [45]. We observe the level repulsion at smaller values of s ($s \ll 1$), where $P(s) \propto s$ and asymptotic decay of $P(s)$ is exponential. The SP distribution is observed within a narrow intermediate

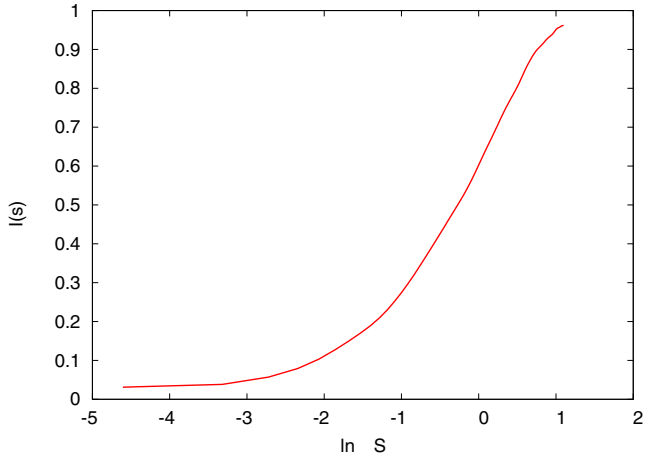

FIG. 5. (Color online) Plot of the integral level-spacing distribution $I(s)$ vs $\ln s$ for $N = 5$.

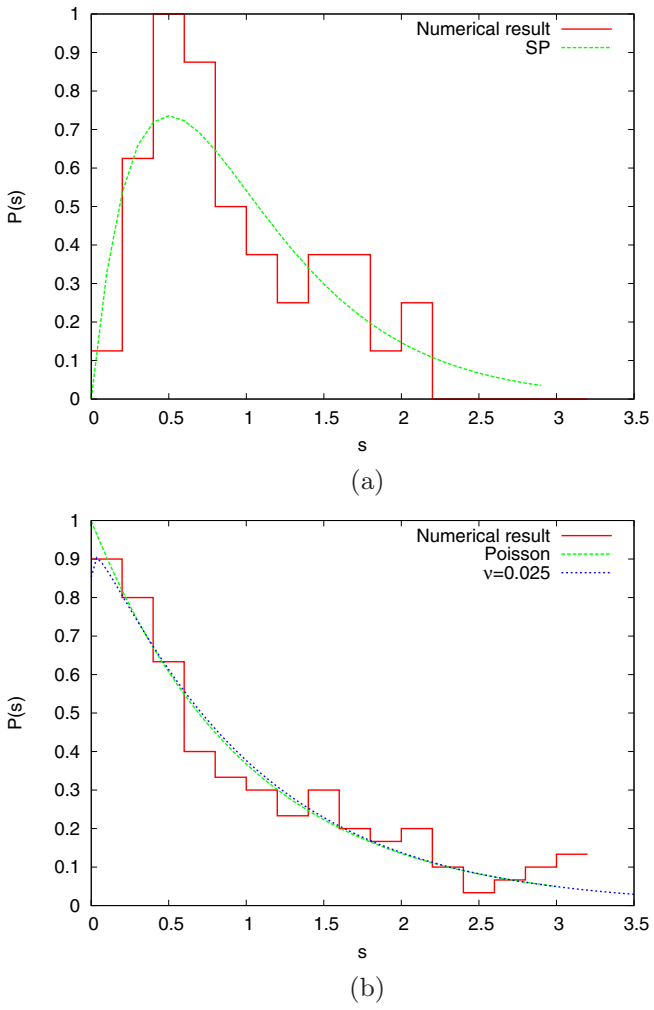

FIG. 6. (Color online) Plot of the $P(s)$ distribution for (a) middle ($40 <$ level < 80) and (b) higher ($850 <$ level < 1000) levels for $N = 5$. The green dashed curve in panel (a) represents the semi-Poisson distribution and that in panel (b) presents the Poisson distribution. The blue dotted curve in panel (b) corresponds to the Brody distribution with the Brody parameter $\nu = 0.025$.

region between the quasidegenerate regime and the completely integrable regime. $P(s)$ distribution for the higher levels are plotted in Fig. 6(b) which is again very similar to Poisson distribution. We again fit the Brody distribution with the histogram and find the Brody parameter $\nu = 0.025$. The observation of the SP distribution and increase in the value of Brody parameter ν clearly manifests the enhanced effect of interatomic correlation with an increase in cluster size. However, we fail to give any physical reason which causes this SP and Poisson statistics. As pointed out earlier, for smaller cluster size only $l = 0$ effective potential is not enough to calculate a sufficient number of levels for the study of $P(s)$ distribution. So the findings of SP statistics may be physically acceptable, the origin of which are not clear to us, or they may be due to the overlap of several l values. Thus to get further insight we significantly change the cluster size to $N = 40$ where only $l = 0$ effective potential is deep enough to support a sufficient number of states for calculation of the

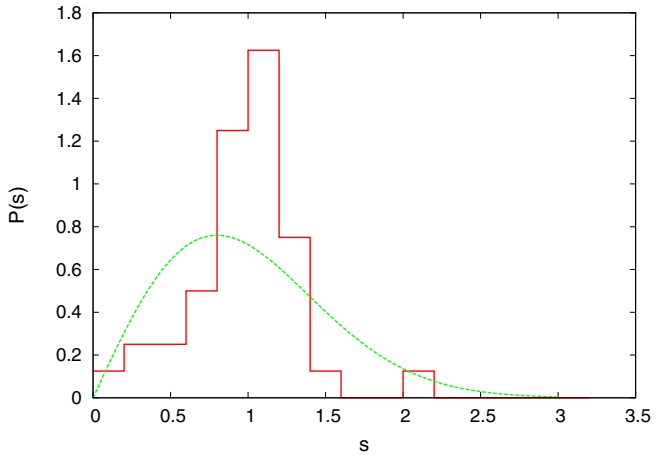

FIG. 7. (Color online) Plot of the nearest neighbor level-spacing distribution $P(s)$ of the higher portion (160–200 levels) of the spectrum of the diffuse van der Waals cluster for $N = 40$. The red smooth histogram represents our numerical result and the green dashed curve represents the Wigner distribution.

$P(s)$ distribution. We plot the $P(s)$ distribution in Fig. 7. We observe a similarity with the Wigner distribution as the very small value of $P(s)$ near $s = 0$ signifies the level repulsion. However, the peak at $s = 1$ overshoots 1. The large peak at $s = 1$ signifies a large accumulation of levels with level spacing $s = 1$. Although we tried to fit the histogram again with the Brody distribution we failed to appropriately fit it. Now it is worth mentioning that Guhr and Weidenmüller [46] proposed a modified uniform spectrum in terms of a deformed GOE, which combines uniform, GOE, and Poisson. As the $P(s)$ distribution of Fig. 7 is quite similar to Figs. 1–3 of Ref. [46], the use of deformed GOE may be an ideal step for future investigation. As Fig. 7 does not match with the Wigner distribution we conclude that the Hamiltonian is not chaotic. However, the deformed GOE-type distribution signifies the system is strictly nonintegrable and exhibits strong interatomic correlation. Thus, it is indeed required to calculate the energy level correlation which we discuss in the following section.

C. Energy level correlation

So far we have considered only the NNSD which is commonly used to characterize the short-range fluctuations in the spectrum. However, in order to confirm our findings of the effect of correlation on the spectral properties and to investigate how the correlation gradually builds in with the increase in cluster size which makes the system too complex, we study the long-range correlations of the spectrum. The level number variance $\Sigma^2(L)$ is the most commonly used observable to characterize correlations between the pair of levels. It mainly determines the long-range fluctuations in the spectrum. It is defined as the average variance of the number of levels in the energy interval containing an average number of L levels and is calculated as

$$\Sigma^2(L) = \langle (N(E+L) - N(E) - L)^2 \rangle, \qquad (16)$$

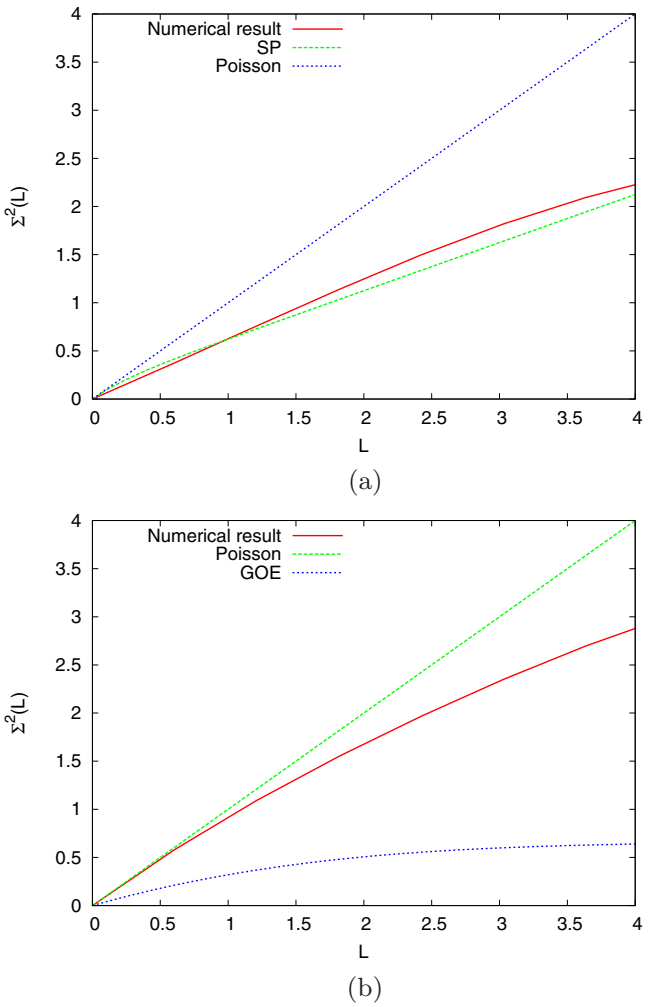

FIG. 8. (Color online) Plot $\Sigma^2(L)$ vs L for the (a) intermediate ($40 <$ level < 80) and higher ($850 <$ level < 1000) part of the spectrum for $N = 5$.

where $\langle\rangle$ represents the average over the energy value E and $N(E)$ determines the number of eigenenergy levels below E. For the uncorrelated Poisson statistics $\Sigma^2(L) = L$, whereas for GOE, $\Sigma^2(L)$ increases logarithmically with L. From the earlier study of level-spacing distribution it has been observed that for $N = 3$ the system exhibits features which are very close to the noninteracting limit. We have also observed the Poisson distribution in the level statistics of higher levels. However, the most interesting observation is the semi-Poisson distribution for the intermediate part of the spectrum for $N = 5$. The corresponding $\Sigma^2(L)$ is plotted in Fig. 8(a). It approximately increases linearly as $L/2$ which is the value of the number variance $\Sigma^2(L)$ of SP distribution. Then we plot $\Sigma^2(L)$ for the higher part of the spectrum in Fig. 8(b). It is approximately proportinal to L indicating that the system is correlated but does not exhibit any level repulsion. This further confirms the findings of the Poisson distribution in the $P(s)$ distribution. For the strongly correlated cluster with $N = 40$ we observe that $\Sigma^2(L)$ approximately increases logarithmically with L (Fig. 9). This feature is close to GOE results. However, there are significant differences between our

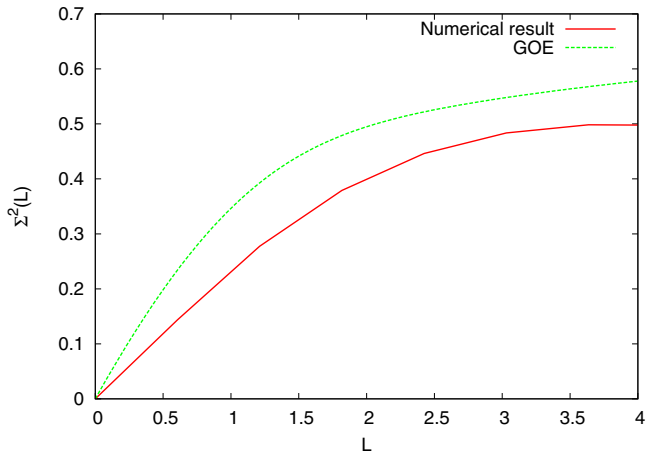

FIG. 9. (Color online) Plot $\Sigma^2(L)$ vs L for the spectrum of the Rb cluster with $N = 40$.

numerical results and the Wigner surmise. This again indicates that the system does not show full chaos although it exhibits strong nonintegrability.

The other important observable to characterize long-range correlation is Δ_3 statistics [24]. Given an energy interval $[\alpha,\alpha + L]$ of length L, it is defined as the least square deviation of the staircase function $\hat{N}(E_i)$ from the best straight line fitting:

$$\Delta_3(\alpha; L) = \frac{1}{L} Min_{A,B} \int_{\alpha}^{\alpha+L} [\hat{N}(E_i) - AE_i - B]^2 dE_i. \tag{17}$$

It is customary to use the average values of $\Delta_3(L)$. Thus Δ_3 statistics, averaged over energy intervals, measures the deviation of the unfolded spectrum from the equidistant spectrum and hence it gives information on the rigidity of spectrum or spectral stiffness. For uncorrelated Poisson spectra $\langle\Delta_3(L)\rangle \propto L$ whereas for Wigner spectra $\langle\Delta_3(L)\rangle \propto \log L$. Our calculated numerical results for $N = 40$ are shown in Fig. 10. Although it looks similar to GOE distribution, it

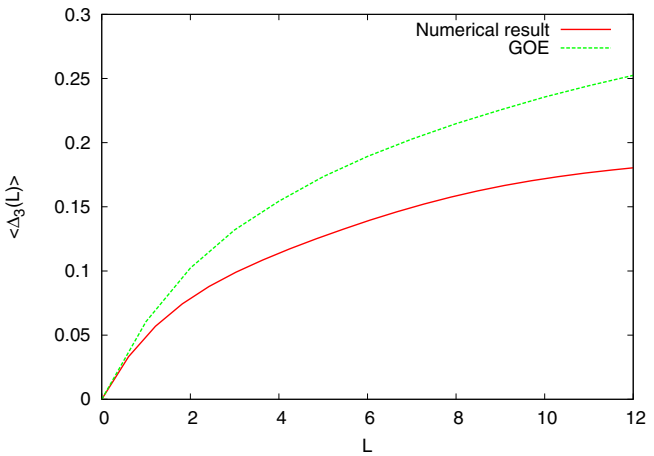

FIG. 10. (Color online) Plot $\langle\Delta_3(L)\rangle$ vs L for the spectrum of the Rb cluster with $N = 40$.

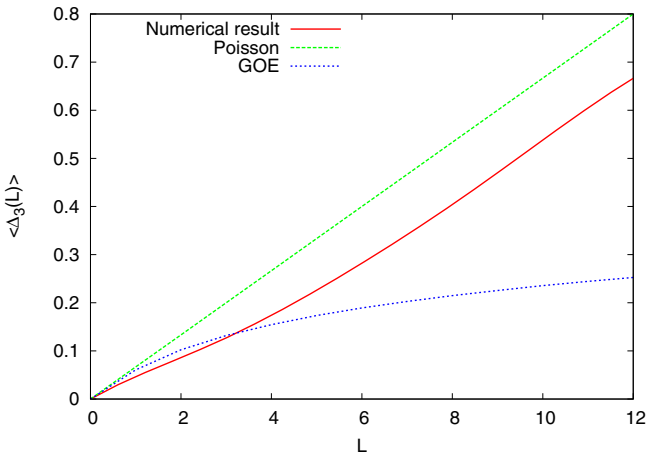

(a)

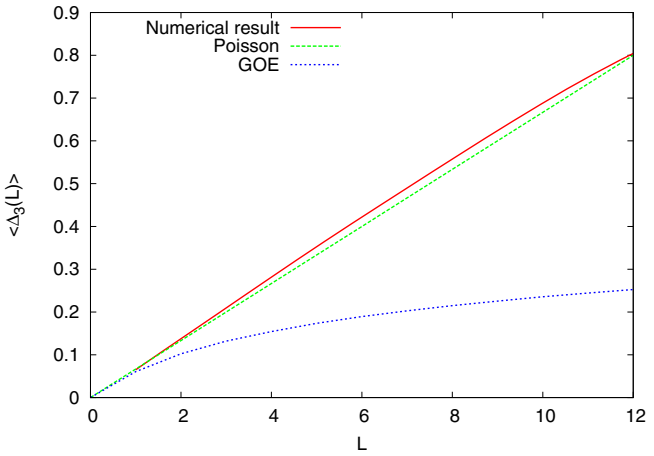

(b)

FIG. 11. (Color online) Plot of $\langle\Delta_3(L)\rangle$ vs L for (a) intermediate (40 < level < 80) and higher part (850 < level < 1000) of the spectrum for $N = 5$.

is significantly lower than the GOE results which confirms our earlier observation for the large cluster. The approach of $\langle\Delta_3(L)\rangle$ towards the GOE behavior is valid only up to $L \approx 2$. The similar kind of observation was made in Fig. 6 of Ref. [46] where deformed GOE behavior is noted in $\langle\Delta_3(L)\rangle$. It indicates that for large cluster size, the levels are strongly correlated, whereas for smaller cluster ($N = 5$), we observe that the $\langle\Delta_3(L)\rangle$ distribution gradually approaches to Poisson as we move upward in the spectrum. For a small intermediate region of the spectrum, $\langle\Delta_3(L)\rangle$ lies between the GOE and Poisson distribution [Fig. 11(a)] whereas for the upper levels it almost perfectly follows the Poisson distribution [Fig. 11(b)] which indicates that the spectrum has turned soft.

D. Quotients of successive spacings

Before concluding the paper, we present in this section, as a test of the observations made in Sec. III B, the results of the analysis of the distribution of quotients of successive level spacings [denoted by $P(r)$], a measure introduced recently, that is independent of the unfolding function and the unfolding procedure [47,48]. Note that in all the analysis

presented in Secs. III B and IIIC, we have employed a sixth-order polynomial for the density of levels for unfolding. The $P(r)$ distribution and the related averages allow for a more transparent comparison with experimental results than the traditional level-spacing distribution and this measure is particularly important for many-body systems as the theory for the eigenvalue (level) densities for these systems is usually not available. In the recent past, this measure was used in analyzing many-body localization [47,49–51] and also in quantifying the distance from integrability on finite-size lattices [52,53]. More recently, using $P(r)$ it is established conclusively

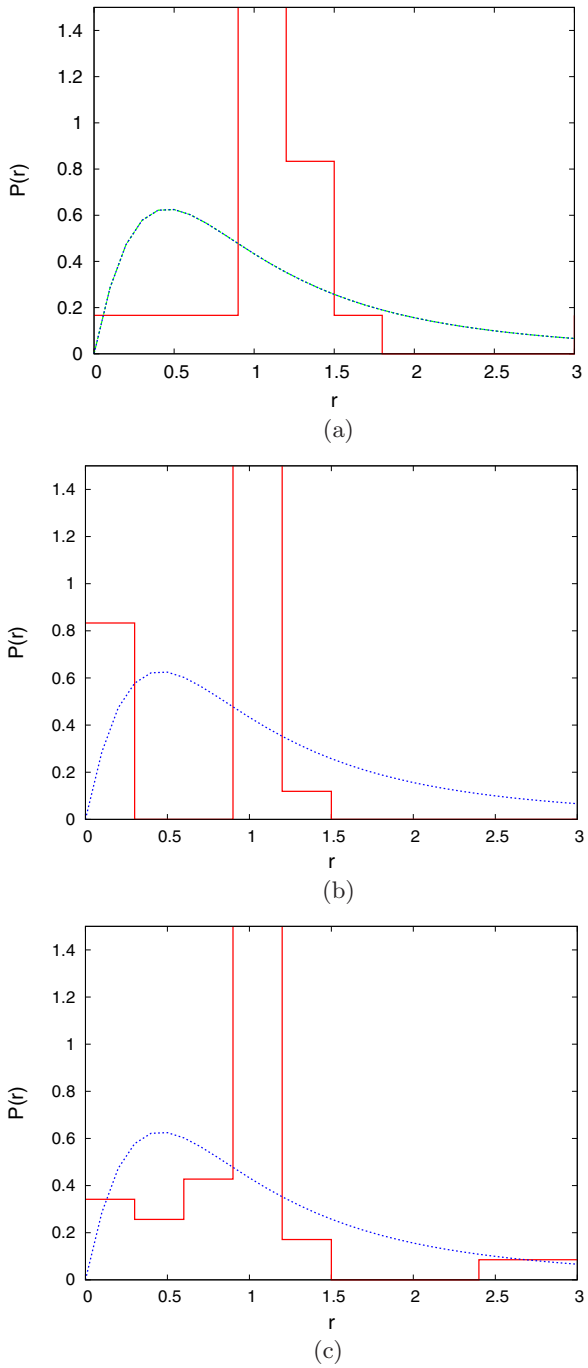

FIG. 12. (Color online) Distribution of the ratio of consecutive level spacings $P(r)$ of the spectrum of diffuse ^{87}Rb for cluster sizes (a) $N = 3$ with lowest 22 levels, (b) $N = 5$ with lowest 30 levels, and (c) $N = 5$ with levels 40–80. Result for GOE (blue curve) is also shown.

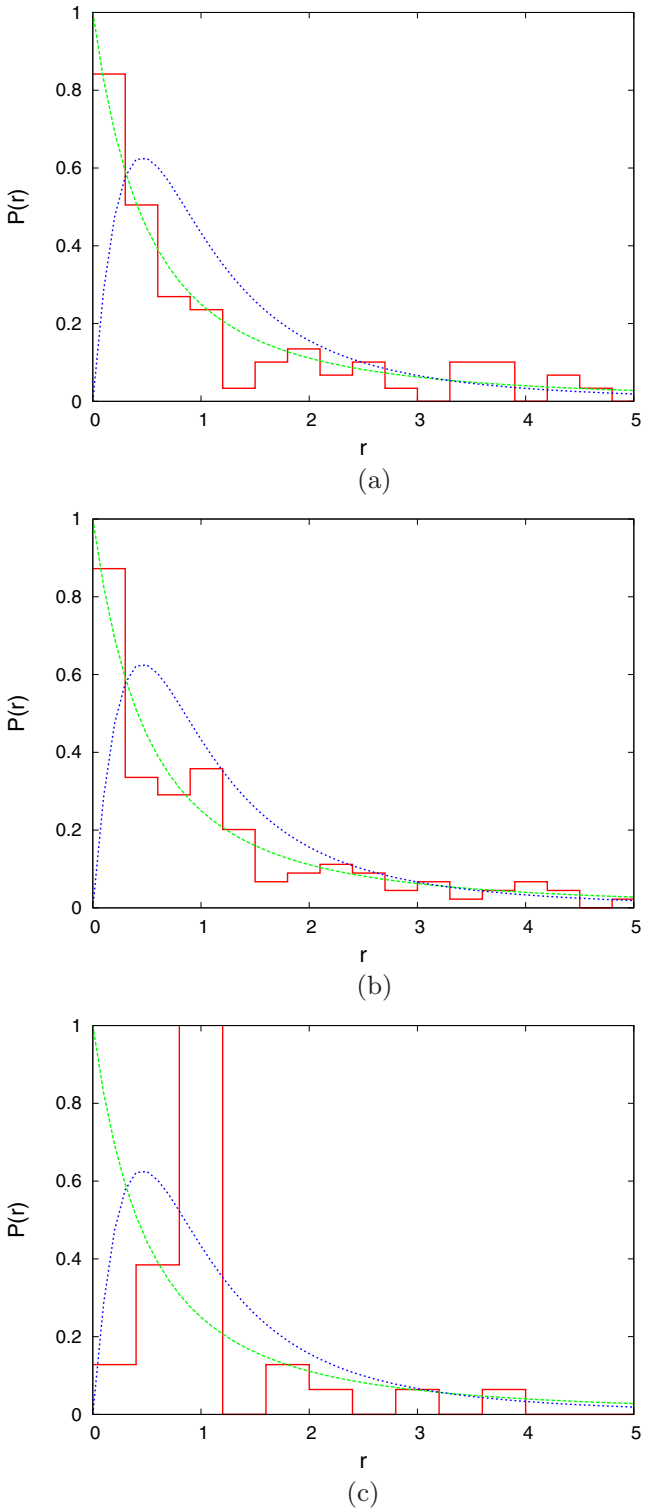

FIG. 13. (Color online) Distribution of the ratio of consecutive level spacings $P(r)$ of the spectrum of diffuse ^{87}Rb for cluster sizes (a) $N = 3$ with levels 300–400, (b) $N = 5$ with levels 850–1000, and (c) $N = 40$ with levels 160–200. Results for Poisson (green curve) and GOE (blue curve) are also shown.

TABLE I. Values of averages $\langle \tilde{r} \rangle$ and $\langle r \rangle$ for various cluster size N.

		$\langle \tilde{r} \rangle$	$\langle r \rangle$
N=3	Levels (1–22)	0.76	1.168
	Levels (300–400)	0.34	204151
N=5	Levels (1–30)	0.48	6.18
	Levels (40–80)	0.64	1.64
	Levels (850–1000)	0.39	144078
N=40	Levels(160–200)	0.76	1.43
GOE		0.5359	1.75
Poisson		0.3863	∞

that embedded random matrix ensembles for many-body systems, generated by random interactions in the presence of a mean field, follow GOE for strong enough two-body interaction [54].

Given an ordered set of the energy levels E_n, the nearest neighbor spacing $s_n = E_{n+1} - E_n$ and the probability distribution of the ratios $r_n = s_n/s_{n-1}$ is $P(r)$ subject to normalization $\int P(r)dr = 1$. If the system is in the integrable domain (described by Poisson NNSD), then the $P(r)$ is given by

$$P_P(r) = \frac{1}{(1+r)^2}, \tag{18}$$

and if the system is chaotic (described by GOE), then the $P(r)$ is given by Wigner-like surmise [48],

$$P_W(r) = \frac{27}{8}\frac{r + r^2}{(1 + r + r^2)^{5/2}}. \tag{19}$$

The average value of r, i.e., $\langle r \rangle$, is 1.75 for GOE and is ∞ for Poisson. It is also possible to consider $\tilde{r}_n = \frac{\min(s_n, s_{n-1})}{\max(s_n, s_{n-1})} = \min(r_n, 1/r_n)$. The average value of $\tilde{r}$, i.e., $\langle \tilde{r} \rangle$, is 0.536 for GOE and 0.386 for Poisson.

Some results for $P(r)$ vs r for the spectrum of the diffuse ^{87}Rb cluster with the same cluster sizes as above *viz.*$N = 3$, 5, and 40, are shown in Figs. 12 and 13. Moreover, we have also calculated the averages $\langle r \rangle$ and $\langle \tilde{r} \rangle$ and results are given in Table I. For $N = 3$ with levels 1–22, there is a peak at $r \sim 1$ as seen from Fig. 12(a). Similarly for levels 300–400, $P(r)$ is close to the Poisson form as shown in Fig. 13(a). These results are consistent with the NNSD results in Figs. 2(a) and 2(b), respectively. In addition, the results for $\langle r \rangle$ and $\langle \tilde{r} \rangle$ given in Table I are also in agreement with these observations. Turning to $N = 5$, with levels 1–30 the $P(r)$ shows peaks at $r \sim 0$ and $r \sim 1$ [see Fig. 12(b)] and for quantifying this structure, it is necessary to derive $P(r)$ that corresponds to the Shnirelman peak. Going to levels 40–80, it is seen from Fig. 12(c) that $P(r)$ exhibits level repulsion with $P(r) \sim 0$ for $r \sim 0$ but the form of $P(r)$ shows clear deviations from the GOE result given by Eq. (19). In order to compare with the conclusion drawn from NNSD in Fig. 6(a), it is necessary to derive the formula for $P(r)$ for pseudointegrable systems (these systems give the semi-Poisson form for NNSD). Turning to levels 850–1000, it is clearly seen from Fig. 13(b) that the $P(r)$ is close to Poisson and this is in complete agreement with NNSD shown in Fig. 6(b). Furthermore, for $N = 40$ the $P(r)$ curve shows level repulsion and it is closer to GOE than to Poisson [see Fig. 13(c)]. In addition, the values of $\langle r \rangle$ and $\langle \tilde{r} \rangle$ (shown in Table I) are close to GOE results. Thus $N = 40$ example exhibits level repulsion as seen in the NNSD result. Combining all these observations, we conclude that the results deduced from NNSD analysis are consistent with those obtained from $P(r)$ analysis and thus the unfolding procedure used in Secs. IIIB and IIIC can be considered to be good.

IV. CONCLUSIONS

Study of energy level statistics plays an important role in elucidating the universal properties of quantum systems. Berry and Tabor conjectured that the eigenenergy levels of a quantum system whose classical dynamics shows integrability, must exhibit the fluctuation property as determined by the uncorrelated Poisson statistics. This is in sharp contrast with the BGS conjecture which asserts that the fluctuation property of energy levels of a quantum system whose classical dynamics should exhibit GOE (or GUE or GSE) statistics. However, complicated quantum many-body systems often lie between these two contrasting conjectures.

Thus the purpose of the present paper is to consider a relatively complex quantum system whose experimental realization is possible. The van der Waals bosonic cluster is such a quantum system which starts to be more and more complex with increase in cluster size. The above-mentioned contrasting conjectures have been examined thoroughly by using various statistical observables like NNSD, level number variance $\Sigma^2(L)$, and the spectral rigidity $\Delta_3(L)$. These observables highlight the short- and long-range correlation, level repulsion, level clustering, and how the features of the above observables crucially depend on the cluster size are also focused. Our detailed numerical analysis reveals that for the smaller cluster when the system is very close to integrability, the Berry and Tabor conjecture is followed. For the large cluster, although we observe similar to the BGS conjecture, deviation occurs. For large clusters the system becomes strongly correlated but does not exhibit true chaos. However, our present study reveals that the deformed GOE type of distribution may be suitable for future investigation.

ACKNOWLEDGMENTS

This work is supported by the DAE-BRNS, government of India, through Grant No. 2009/37/23/BRNS/1903. S.K.H. acknowledges the Council of Scientific and Industrial Reaserch (CSIR), India for a senior research fellowship through NET [Grant No. 08/561(0001)/2010-EMR-1]. N.D.C. acknowledges financial support from the University Grants Commission (UGC), India [Grant No. F.40-425/2011 (SR)]. S.K.H. also acknowledges hospitality of the Maharaja Sayajirao University of Baroda, Vadodara, India during a recent visit for this work. B.C. would like to thank the FAPESP (Brazil) for providing financial assistance for her visit to the Universidade de São Paulo, Brazil, where the preliminary part of this work had been started.

[1] T. Kramer *et al*., Nature (London) **440**, 315 (2006).
[2] E. A. Donley *et al*., Nature (London) **417**, 529 (2002).
[3] C. H. Chin, T. Kraemer, M. Mark, J. Herbig, P. Waldburger, H. C. Nagerl, and R. Grimm, Phys. Rev. Lett. **94**, 123201 (2005).
[4] M. H. Anderson, J. R. Ensher, M. R. Matthews, C. E. Wieman, and E. A. Cornell, Science **269**, 198 (1995).
[5] P. K. Debnath, B. Chakrabarti, T. K. Das, and S. Canuto, J. Chem. Phys. **137**, 014301 (2012).
[6] M. V. Berry and M. Tabor, Proc. R. Soc. London A **356**, 375 (1977).
[7] O. Bohigas, M.-J. Giannoni, and C. Schmit, Phys. Rev. Lett. **52**, 1 (1984).
[8] G. Casati, F. Valz-Gris, and I. Guarneri, Lett. Nuovo Cimento Soc. Ital. Fis. **28**, 279 (1980).
[9] F. Haake, *Quantum Signatures of Chaos* (Springer, New York, 2010).
[10] T. H. Seligman, J. J. M. Verbaarschot, and M. R. Zirnbauer, Phys. Rev. Lett. **53**, 215 (1984).
[11] T. Zimmermann, H.-D. Meyer, H. Köppel, and L. S. Cederbaum, Phys. Rev. A **33**, 4334 (1986).
[12] G. Tanner, K. Richter, and J.-M. Rost, Rev. Mod. Phys. **72**, 497 (2000).
[13] J. Sakhr and N. D. Whelan, Phys. Rev. A **62**, 042109 (2000).
[14] T. A. Brody *et al*., Rev. Mod. Phys. **53**, 385 (1981).
[15] V. K. B. Kota, Phys. Rep. **347**, 223 (2001).
[16] J. M. G. Gómez, K. Kar, V. K. B. Kota, R. A. molina, A. Relaño and J. Retamosa, Phys. Rep. **499**, 103 (2011).
[17] L. Muñoz, E. Faleiro, R. A. Molina, A. Relaño, and J. Retamosa, Phys. Rev. E **73**, 036202 (2006).
[18] R. J. Leclair, R. U. Haq, V. K. B. Kota, and N. D. Chavda, Phys. Lett. A **372**, 4373 (2008).
[19] N. D. Chavda, V. Potbhare, and V. K. B. Kota, Phys. Lett. A **311**, 331 (2003).
[20] M. Vyas, V. K. B. Kota, N. D. Chavda, and V. Potbhare, J. Phys. A, Math. Theor. **45**, 265203 (2013); arXiv:1010.6054.
[21] B. Chakrabarti, A. Biswas, V. K. B. Kota, K. Roy, and S. K. Haldar, Phys. Rev. A **86**, 013637 (2012).
[22] K. Roy, B. Chakrabarti, A. Biswas, V. K. B. Kota, and S. K. Haldar, Phys. Rev. E **85**, 061119 (2012).
[23] K. Roy, B. Chakrabarti, and V. K. B. Kota, Phys. Rev. E **87**, 062101 (2013).
[24] M. L. Mehta, *Random Matrices* (Academic Press, New York, 1991).
[25] B. Chakrabarti, T. K. Das, and P. K. Debnath, Phys. Rev. A **79**, 053629 (2009).
[26] S. K. Haldar, B. Chakrabarti, and T. K. Das, Phys. Rev. A **82**, 043616 (2010).
[27] P. K. Debnath and B. Chakrabarti, Phys. Rev. A **82**, 043614 (2010).
[28] A. Biswas, T. K. Das, L. Salasnich, and B. Chakrabarti, Phys. Rev. A **82**, 043607 (2010).
[29] A. Biswas, B. Chakrabarti, T. K. Das, and L. Salasnich, Phys. Rev. A **84**, 043631 (2011).
[30] S. K. Haldar, B. Chakrabarti, T. K. Das, and A. Biswas, Phys. Rev. A **88**, 033602 (2013).
[31] S. K. Haldar, P. K. Debnath, and B. Chakrabarti, Eur. Phys. J. D **67**, 188 (2013).
[32] T. K. Das, B. Chakrabarti, and S. Canuto, J. Chem. Phys. **134**, 164106 (2011).
[33] S. K. Haldar, B. Chakrabarti, and T. K. Das, Few-Body Systems **53**, 283 (2012).
[34] T. K. Das and B. Chakrabarti, Phys. Rev. A **70**, 063601 (2004).
[35] T. K. Das, S. Canuto, A. Kundu, and B. Chakrabarti, Phys. Rev. A **75**, 042705 (2007).
[36] T. K. Das, A. Kundu, S. Canuto, and B. Chakrabarti, Phys. Lett. A **373**, 258 (2009).
[37] J. L. Ballot and M. Fabre de la Ripelle, Ann. Phys. (NY) **127**, 62 (1980).
[38] M. Fabre de la Ripelle, Ann. Phys. (NY) **147**, 281 (1983).
[39] M. Fabre de la Ripelle, Few-Body Syst. **1**, 181 (1986).
[40] C. J. Pethick and H. Smith, *Bose-Einstein Condensation in Dilute Gases* (Cambridge University Press, Cambridge, 2001).
[41] T. K. Das, H. T. Coelho, and M. Fabre de la Ripelle, Phys. Rev. C **26**, 2281 (1982).
[42] S. Bhattacharyya, T. K. Das, and B. Chakrabarti, Phys. Rev. A **88**, 053614 (2013).
[43] O. Bohigas and M.-J. Giannoni, in *Mathematical and Computational Methods in Nuclear Physics*, Vol. 209 of Lecture Notes in Physics, edited by J. S. Dehesa, J. M. G. Gomez, and A. Polls (Springer, New York, 1984).
[44] A. I. Shnirelman, Usp. Mat. Nauk **30**, 265 (1975); A. I. Shnirelman, in *KAM Theory and Semiclassical Approximations to Eigenfunctions*, edited by V. F. Lazutkin (Springer, Berlin, 1993), addendum.
[45] A. M. García-García, Phys. Rev. E **72**, 066210 (2005).
[46] T. A. Guhr and H. A. Weidenmüller, Ann. Phys. (NY) **193**, 472 (1989).
[47] V. Oganesyan and D. A. Huse, Phys. Rev. B **75**, 155111 (2007).
[48] Y. Y. Atas, E. Bogomolny, O. Giraud, and G. Roux, Phys. Rev. Lett. **110**, 084101 (2013).
[49] V. Oganesyan, A. Pal, and D. A. Huse, Phys. Rev. B **80**, 115104 (2009).
[50] A. Pal and D. A. Huse, Phys. Rev. B **82**, 174411 (2010).
[51] S. Iyer, V. Oganesyan, G. Refael, and D. A. Huse, Phys. Rev. B **87**, 134202 (2013).
[52] C. Kollath, G. Roux, G. Biroli, and A. M. Läuchli, J. Stat. Mech. (2010) P08011.
[53] M. Collura, H. Aufderheide, G. Roux, and D. Karevski, Phys. Rev. A **86**, 013615 (2012).
[54] N. D. Chavda and V. K. B. Kota, Phys. Lett. A **377**, 3009 (2013).